



# Improvement of Perovskite $\text{CH}_3\text{NH}_3\text{PbI}_3$ Films on Crystallization for Efficient Perovskite Solar Cells with Low-Temperature Anti-solvent Approach

Qi Wang<sup>1</sup> · Junjie Jiang<sup>1,2</sup> · Xiaoshan Wu<sup>1,2</sup> · Fengming Zhang<sup>1</sup>

Received: 5 August 2023 / Accepted: 4 October 2023 / Published online: 1 November 2023  
© The Minerals, Metals & Materials Society 2023

## Abstract

The effect of anti-solvent IPA (isopropyl alcohol,  $\text{C}_3\text{H}_8\text{O}$ ) treatment at low temperatures on the crystallization of perovskite  $\text{CH}_3\text{NH}_3\text{PbI}_3$  (MAPbI<sub>3</sub>) films has been investigated. It has been indicated that both the grain size in the films and the crystalline quality of the films are improved by using anti-solvent IPA treatment at 250 K, in comparison with the treatment at 300 K (room temperature). The improvement on the film crystalline quality has also been demonstrated from the performance enhancement of fabricated solar cells, as indicated by the power conversion efficiency (PCE) of 19.65% and 17.2% for the cells with films treated at 250 K and 300 K, respectively.

**Keywords** Perovskite · solar cells · low temperature anti-solvent · crystallization

## Introduction

The one-step spin-coating process is widely used as a mainstream method for preparing organic–inorganic hybrid metal halide perovskite solar cells (PSCs).<sup>1–6</sup> By this process, the nucleation rate in preparing  $\text{CH}_3\text{NH}_3\text{PbI}_3$  (MAPbI<sub>3</sub>) films is excessively low, causing the precursors to preferentially grow on existing nuclei instead of forming new ones.<sup>7–10</sup> The low nucleation rate is more favored for the growth of larger grain sizes. On the other hand, the low growth rate due to the low mobility results in a film surface with a haphazard accumulation of forked crystals, high roughness, and a significant number of pores, which severely limit the performance of the device. The anti-solvent-assisted one-step spin-coating method is highly effective in improving the crystallization process of MAPbI<sub>3</sub>.<sup>11–13</sup> The introduction of an anti-solvent can significantly increase the mobility of the radicals, resulting in a notable improvement in the film's surface morphology and overall device performance. Consequently, it has

become the most widely employed approach for preparing PSCs. The characteristics of the anti-solvent play a crucial role in the crystallization process of perovskite materials, making it a prominent research area. For example, Mai's team utilized ethyl acetate in combination with polymethyl methacrylate as a green, simple, and environmentally friendly anti-solvent intermediate. This approach facilitates the internal growth of perovskite grains while simultaneously passivating interface and bulk defects, leading to a reduction in non-radiative recombination.<sup>14</sup> By employing MABr dissolved in ethanol (MABr-Eth) as an anti-solvent to treat perovskite films, Wei's group has successfully enhanced both the grain size and the crystallinity of the perovskite material while passivating surface defects. Furthermore, the interaction between MABr and  $\text{PbI}_2$ , which is produced during the perovskite decomposition by ethanol washing, prevents perovskite loss and improves light absorption of the films. As a result, the best power conversion efficiency (PCE) of the prepared inverted-monolithic heterojunction device is 21.53%.<sup>15</sup> Li's group used a mixture of ethyl acetate and various polar alcohols as the anti-solvent, which effectively enhanced the migration of halogen atoms while altering the crystallographic orientation of the perovskite complexes.<sup>16</sup> Moon's group reported an interesting approach, in which the substrates were first coated with ( $\text{PbI}_2 + \text{MAI}$ ) films, and then dipped in an anti-solvent bath of 0°C (273 K) before annealing for perovskite film growth.<sup>17</sup> Yang and

✉ Fengming Zhang  
fmzhang@nju.edu.cn

<sup>1</sup> National Laboratory of Solid State Microstructures and School of Physics, Nanjing University, Nanjing 210093, China

<sup>2</sup> Institute of Materials Engineering, Nantong 226019, China

Hong's group presented the work on the determination of the optimal treatment time for the anti-solvent at different environmental temperatures between  $22^\circ\text{C}$  and  $31^\circ\text{C}$  in a glove box by monitoring the performance of solar cells.<sup>18</sup> Niu and Zhao's group investigated the effects of a hot substrate at different temperatures between  $30^\circ\text{C}$  and  $70^\circ\text{C}$  on the crystallization process and properties of mixed-ion perovskite layers.<sup>19</sup>

It seems that, for the use of an anti-solvent, a compromise between better film quality and small grain size due to a higher nucleation rate has to be made. As we know, the synthesis of perovskite  $\text{CH}_3\text{NH}_3\text{PbI}_3$  is a practical process of solid phase reaction. The key stages consist of nucleation and following grain growth. The role of the anti-solvent is to enhance the nucleation rate before the growth. However, temperature is another important factor for monitoring the reaction. In the low temperature range, the nucleation rate decreases with decreasing temperature. The competition between lower temperature and anti-solvent determines the final nucleation rate. Dai's group reported a good trial,<sup>20</sup> when they studied the effect of the anti-solvent (a mixture of diethyl, chlorobenzene, and toluene) with temperature between  $0^\circ\text{C}$  and  $30^\circ\text{C}$ . However, it is believed that the temperature effect below the room temperature range is quite interesting and helpful to the community. In this work, firstly, pure IPA (isopropyl alcohol,  $\text{C}_3\text{H}_8\text{O}$ ) was used as the anti-solvent. Secondly, experiments with temperatures of

300 K, 250 K, and 200 K, respectively, for the anti-solvent IPA (isopropyl alcohol,  $\text{C}_3\text{H}_8\text{O}$ ) were conducted for the preparation of  $\text{MAPbI}_3$  films. With success for temperatures of 300 K and 250 K, the experiment for the anti-solvent IPA at 200 K failed due to the very high viscosity of the IPA at that temperature. The characterization of the structures and relevant physical properties of the films are presented. Solar cells with films prepared by using the anti-solvent IPA at 250 K and 300 K have been fabricated and the corresponding performance of the cells has been characterized.

## Experimental

Commercial glass substrates with an FTO coating were processed by washing steps, including rinsing with deionized water, acetone, and ethanol for 15 min each. The substrates were then dried by using nitrogen blowing and treated in a UV ozone oven for 15 min. After a layer of  $\text{SnO}_2$  coating was prepared on the cleaned substrates by using spin-coating of  $\text{SnO}_2$  solution (with deionized water and  $\text{SnO}_2$  at a volume ratio of 1:5) at 4000 rpm for 30 s, the substrates were annealed at  $150^\circ\text{C}$  for 30 min for the required electron transport layer (ETL) formation.

For the synthesis of the  $\text{MAPbI}_3$  films, the one-step spin-on coating method was employed in a nitrogen-filled glove box. The main processes are shown in Fig. 1. The perovskite

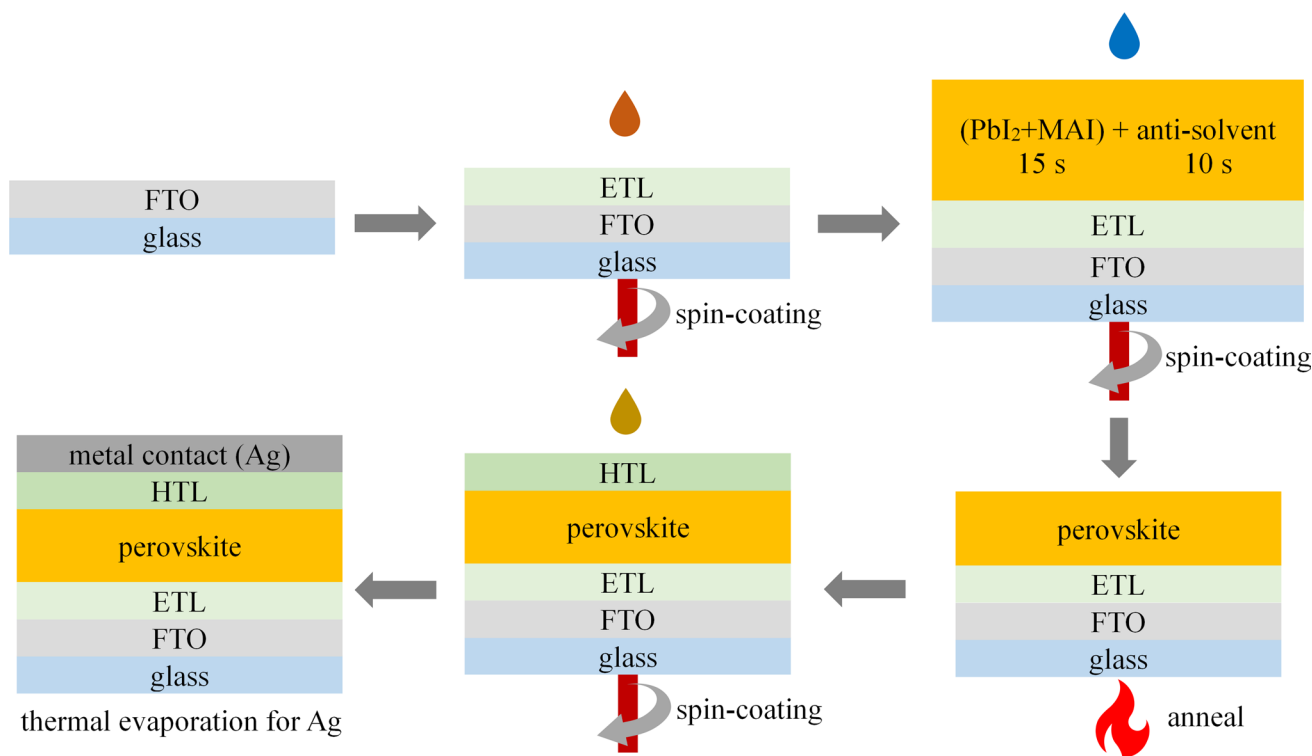


**Fig. 1** Schematic of the fabrication processes for  $\text{MAPbI}_3$  films and solar cells.

solution consisted of 46 mg  $\text{PbI}_2$  and 159 mg MAI dissolved in 600 mg of dimethylformamide, and 78 mg of methylsulfoxide. After stirring for more than 6 h, the solution was ready for film coating. With a volume of 80  $\mu\text{L}$  of the solution dripped onto the substrates with ETL, the spin-coating process was initiated at settings of 4000 rpm spin speed and 25 s time duration. After the first 15 s during the spinning of 25 s, anti-solvent IPA (isopropyl alcohol,  $\text{C}_3\text{H}_8\text{O}$ ) with different temperatures (250 K and 300 K) was dripped onto the different samples, which were subsequently annealed at 100°C for 30 min.

To fabricate solar cells with the films treated by using different temperatures of the anti-solvent IPA, the films were coated with a solution of spiro-OMeTAD (for the hole transport layer) and chlorobenzene (in the ratio of 72.3 mL to 1 mL), supplemented by 28.8  $\mu\text{L}$  of 4-tert-butylpyridine, 17.5  $\mu\text{L}$  of a stock solution of 520 mg/mL lithium bis (trifluoromethyl sulphonyl) imide in acetonitrile, and 29  $\mu\text{L}$  of 520 mg/mL tris (2-(1H-pyrazol-yl)- 4-tert-butylpyridine) cobalt (III) bis (trifluoromethyl sulphonyl) imide in acetonitrile. This solution was spin-coated at 4000 rpm for 30 s, followed by the deposition of an 80-nm Ag film using thermal evaporation.

The characterization focused on the films treated with the anti-solvent at 250 K and 300 K, while the performance

analysis of the solar cells was based on the corresponding films.

X-ray diffraction (XRD; D/max-RB; Rigaku) data were collected in the angular range of  $10^\circ < 2\theta < 90^\circ$ , with step angle of  $0.02^\circ$ .  $\text{CuK}\alpha$  radiation ( $\lambda = 0.1541 \text{ nm}$ ) was used for the measurements. Scanning electron microscope (SEM) images and energy-dispersive x-ray spectroscopy (EDS) were obtained (SIGMA 500/VP; ZEISS). Current–voltage measurements were conducted using a Keithley 2400 instrument under AM 1.5 G illumination ( $1000 \text{ W/m}^2$ ) from a solar simulator (Oriel Solar 3A Class AAA, 94023 A; Newport). Photoluminescence (PL; LabRAM HR Evolution; Horiba) was performed using a 633-nm diode laser excitation source.

## Results and Discussion

Figure 2a shows optical microscope observation images of the film surfaces treated with the anti-solvent at 300 K (labeled Film A) and at 250 K (labeled Film B), respectively. The surfaces of both Film A and Film B obviously exhibit a uniform and flat appearance, resembling a black mirror-like state, a typical feature of the anti-solvent approach. The grain structures of Film A and Film B were investigated

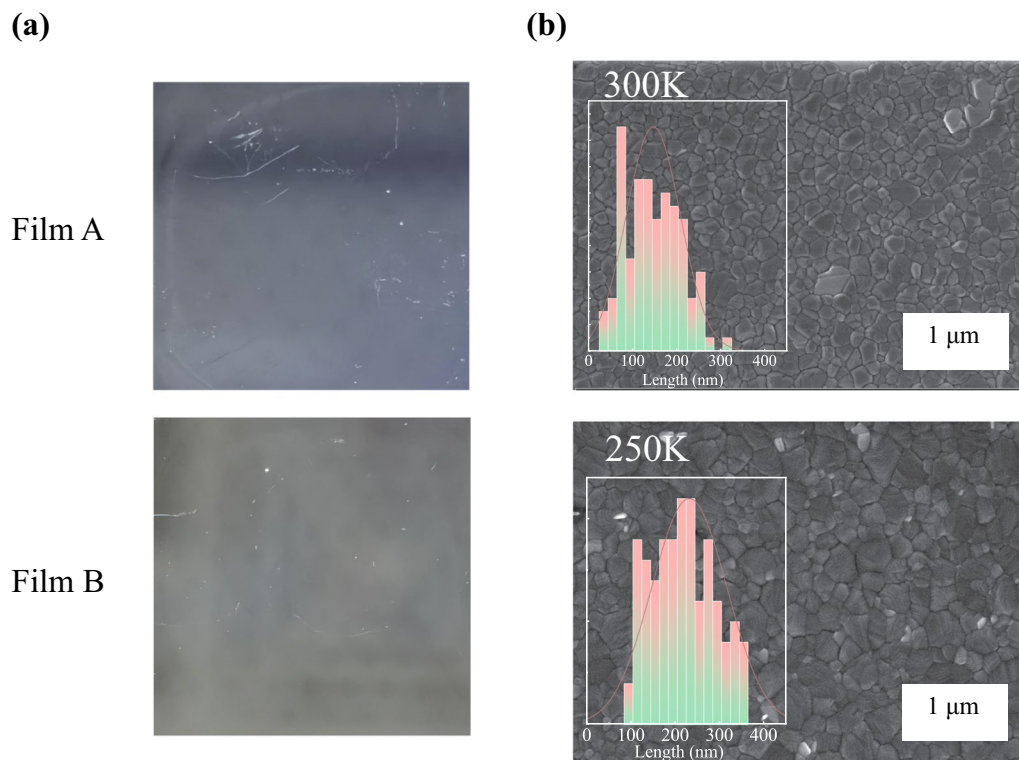


**Fig. 2** (a) Perovskite films ( $1.5 \text{ cm} \times 1.5 \text{ cm}$ ) prepared with the anti-solvent at 300 K (Film A) and 250 K (Film B), respectively; (b) SEM images of the grain sizes of perovskite films treated with the anti-solvent of 250 K and 300 K.

by SEM. As depicted in Fig. 2b, the grains in both films are well-defined and closely aligned, with an obvious larger average grain size in Film B compared with that in Film A. In fact, as discussed in the Introduction, the use of an anti-solvent can quickly remove some of the solvent in the coated films, which will enhance the nucleation rate and assist the crystalline quality of the perovskite films during the annealing process. However, the enhanced nucleation rate will increase the density of the nucleation, causing a small grain size in the films. The larger grain size in Film B than in Film A demonstrates the success of the approach by lowering the initial temperature of the anti-solvent to keep the nucleation rate low for the larger grain size, while the better crystalline quality of the grains is maintained.

The structures and optoelectronic properties of the films have been further investigated. Figure 3a presents the XRD results, in which the peaks at 14.08°, 28.40°, and 31.84° correspond to the [110], [220], and [310] crystal planes of the tetragonal phase MAPbI<sub>3</sub>, respectively.<sup>21</sup> The XRD patterns reveal that the diffraction intensity of Film B slightly increases in comparison with that of Film A, indicating an enhanced crystallinity in Film B. Moreover, the XRD spectra of both Film A and Film B exhibit a prominent PbI<sub>2</sub> peak at 12.5°, which means that some mixed phase of PbI<sub>2</sub> exists in the films. EDS analysis was conducted to determine the comprehensive I-to-Pb ratios in the films. Theoretically, a ratio of 3 should be the perfect value for the ideal structure. However, any deviation of the composition of the stoichiometry in the films could cause a mixed phase. As shown in the inset in Fig. 3a, the ratio of I/Pb in Film B (2.77) is higher than that in Film A (2.68), indicating a composition closer to the ideal value in Film B

compared with Film A. As is known, both MAI and PbI<sub>2</sub> are soluble in an anti-solvent, although the solubility is low. During the spin-coating process, small portions of MAI and PbI<sub>2</sub> become dissolved in the anti-solvent. Due to the higher solubility of MAI compared to PbI<sub>2</sub>, more MAI is dissolved in the process, resulting an excess of PbI<sub>2</sub> in the films, although the stoichiometric composition in the original precursor solution is the ideal one. Based on this, the observed behavior can be reasonably understood. The enhanced crystallinity in Film B is caused by the less excessive PbI<sub>2</sub> in the film, as the decreased temperature of the anti-solvent for preparing Film B reduced the loss of MAI due to its lower solubility at the lower temperature. Therefore, more MAI reacting with PbI<sub>2</sub> occurs in Film B, reducing the excess of PbI<sub>2</sub>.

Figure 3b illustrates the absorption spectra of the films. It can be seen that the absorption spectra of both Film A and Film B are almost identical, indicating the same optical properties. Tauc's equation was employed to calculate the optical band gap of the films using the fitted absorption spectrum:

$$(\alpha h\nu)^n = B(h\nu - E_g) \quad (1)$$

where  $\alpha$  represents the absorption coefficient,  $h$  is Planck's constant,  $\nu$  represents the frequency of light, and  $E_g$  denotes the band gap. The value of  $n$  is taken as 1/2 for indirect band-gap semiconductors and 2 for direct band-gap semiconductors. Referring to Fig. 3b, we consider  $(\alpha h\nu)^2$  as the vertical coordinate and  $h\nu$  as the horizontal coordinate. By conducting linear regression analysis on the linear region, the intercept of the fitted line on the  $x$ -axis represents the band gap value. The optical band gaps of Film A and Film

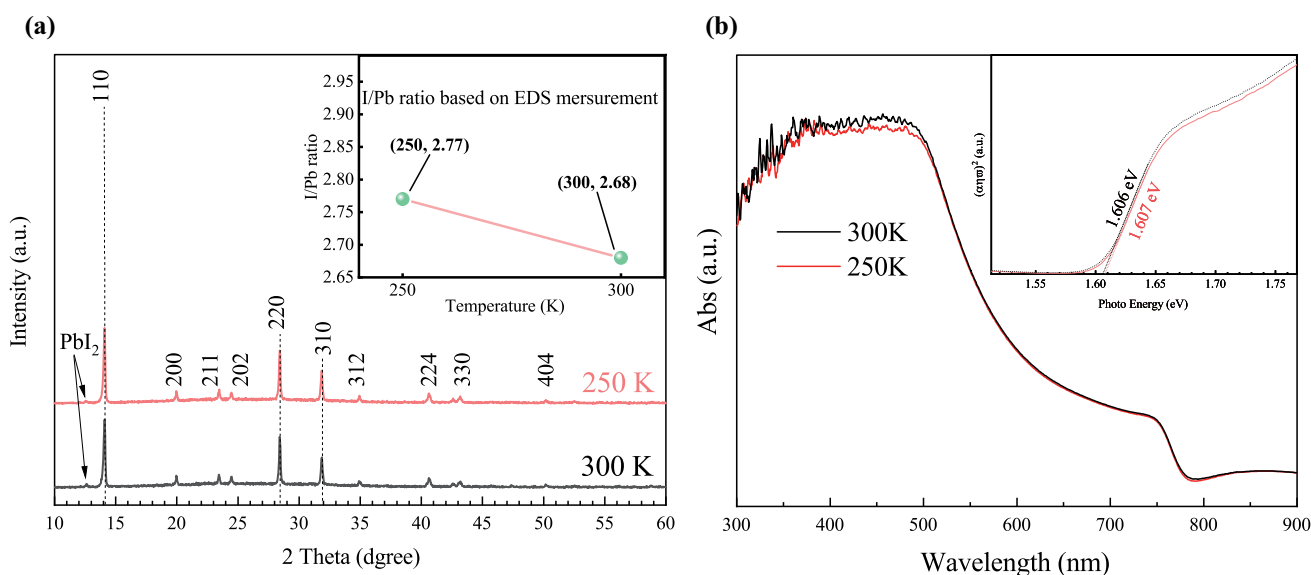


**Fig. 3** (a) XRD spectra and EDS patterns of the perovskite films treated at 300 K (Film A) and 250 K (Film B) inset indicates that the I/Pb ratio in Film B is closer to the ideal value of 3 than that in Film A; (b) absorption spectrum; inset optical band gap fitting.

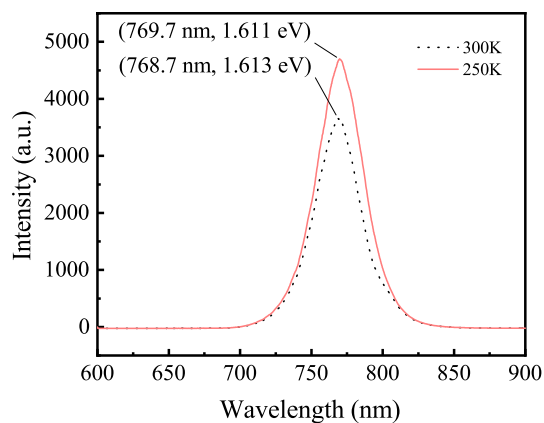


**Fig. 4** Steady-state PL spectra of films on bare glass substrates with the anti-solvent at 300 K (Film C) and at 250 K (Film D).

B are approximately 1.606 eV and 1.607 eV, respectively, showing nearly identical values.

PL spectroscopy is a commonly employed technique for assessing the photoelectric properties of films.<sup>22–25</sup> In general, when considering perovskite films without carrier collection layers, a higher PL intensity indicates a lower presence of non-radiative recombination processes within the films. This implies that there are fewer defects and higher overall film quality.<sup>22,26,27</sup> For the purpose of investigation with PL spectra, Film C and Film D were prepared on bare glass substrates with the same corresponding conditions of Film A and Film B, respectively. Figure 4 illustrates the steady-state PL spectra of Film C and Film D. With an excitation wavelength of 633 nm for the PL measurement, the band gap was determined, and a slight deviation from that was obtained through the absorption

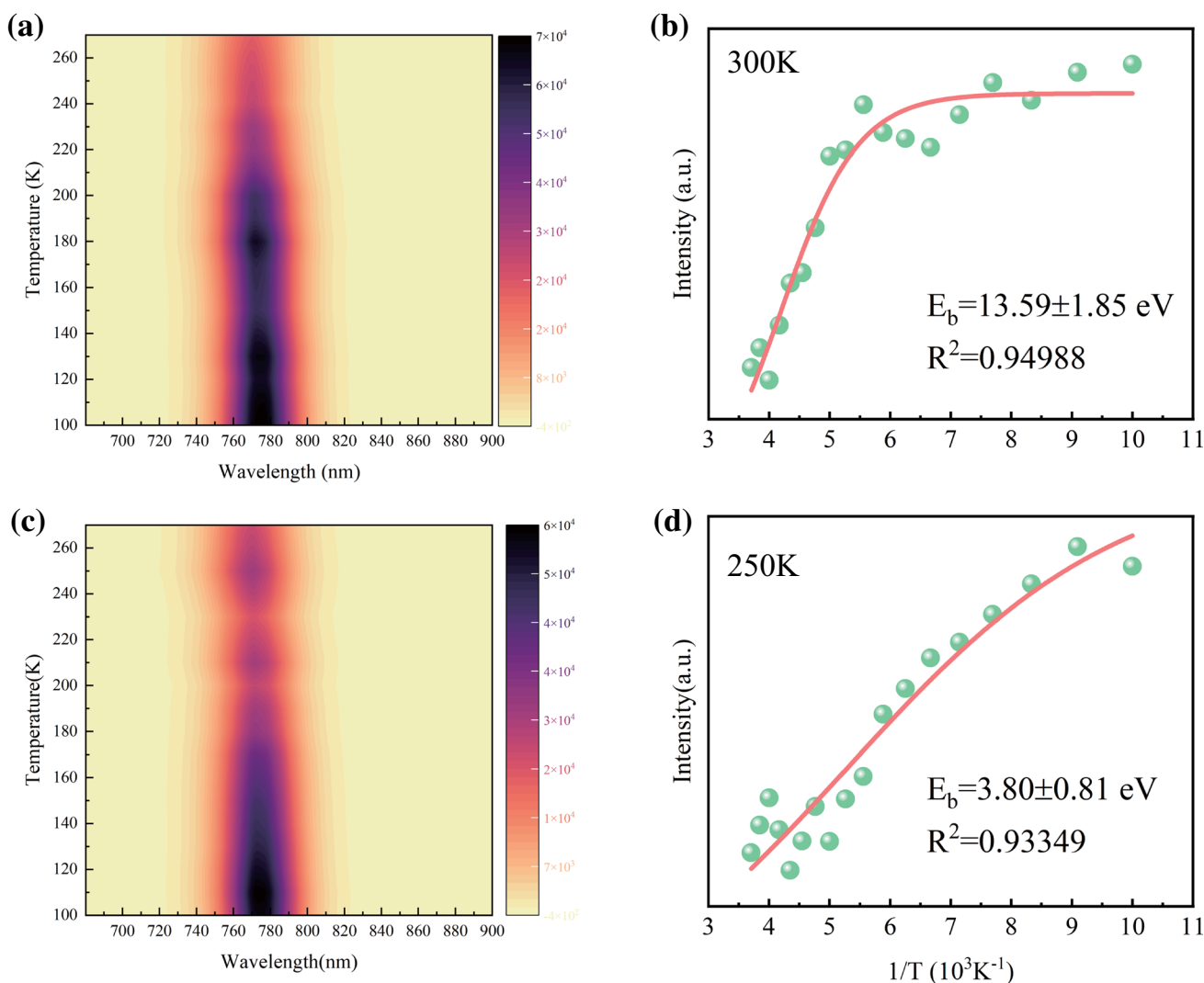


**Fig. 5** Temperature-dependent PL color diagram of Film C (a) and Film D (c); PL intensity versus inverse temperature of Film C (b) and Film D (d) (Color figure online).

spectrum fitting. However, this difference falls within the acceptable range of error and demonstrates a consistent trend. In terms of PL intensity, Film D exhibits a higher value than Film C. Consistently, as the anti-solvent treatment at 250 K, in comparison with at 300 K, can enhance the crystallinity of the film and increase the average grain size, the result is a higher PL intensity.

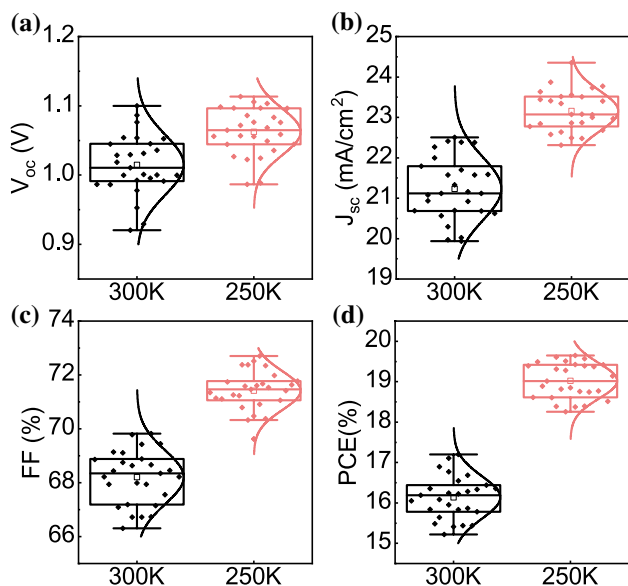


**Fig. 6** Cell performance statistics of  $V_{oc}$  (a),  $J_{sc}$  (b), FF (c), and PCE (d) of 27 cells with anti-solvent at 300 K or 250 K in film preparation. The hollow dots represent the mean values, the box edges represent the standard deviations, the whiskers represent the maximum and minimum of the distributions, and the central horizontal line represents the median.

In general, the rate of carrier recombination is directly proportional to the exciton binding energy. In the context of perovskite solar cell devices, a lower exciton binding energy facilitates the dissociation of excitons into free carriers and their extraction, thereby leading to improved device performance. We conducted an analytical study and obtained a plot of PL intensity against the inverse of temperature ( $1/T$ ), as depicted in Fig. 5. The relationship between PL intensity and temperature can be effectively fitted using the Arrhenius equation<sup>28</sup>:

$$I(T) = \frac{I_0}{1 + Ae^{-E_b/k_b T}} \quad (2)$$

where  $I(T)$  and  $I_0$  represent the PL intensity at temperatures  $T$  K and 0 K, respectively,  $E_b$  denotes the exciton binding energy, and  $k_b$  is the Boltzmann constant. By performing a fitting analysis, it was determined that the exciton binding energy of Film C was  $13.59 \pm 1.85$  meV, whereas that of Film D experiences a significant decrease to  $3.80 \pm 0.81$  meV. It is important to note that the method of calculating the exciton binding energy through variable-temperature PL has certain limitations, such as not accounting for changes in the exciton binding energy resulted from phase transitions during the temperature variations. Nevertheless, it can be qualitatively concluded that Film D exhibits a considerably reduced exciton binding energy compared to Film C.

Finally, two groups of sample films with the same preparation conditions as Film A and Film B were fabricated for solar cell devices with the structure of FTO/SnO<sub>2</sub>/perovskite/Spiro-OMeTAD/Ag, labeled group of Cells A and group of Cells B, correspondingly. The statistics of the device parameters obtained from 27 cells of each group are presented in

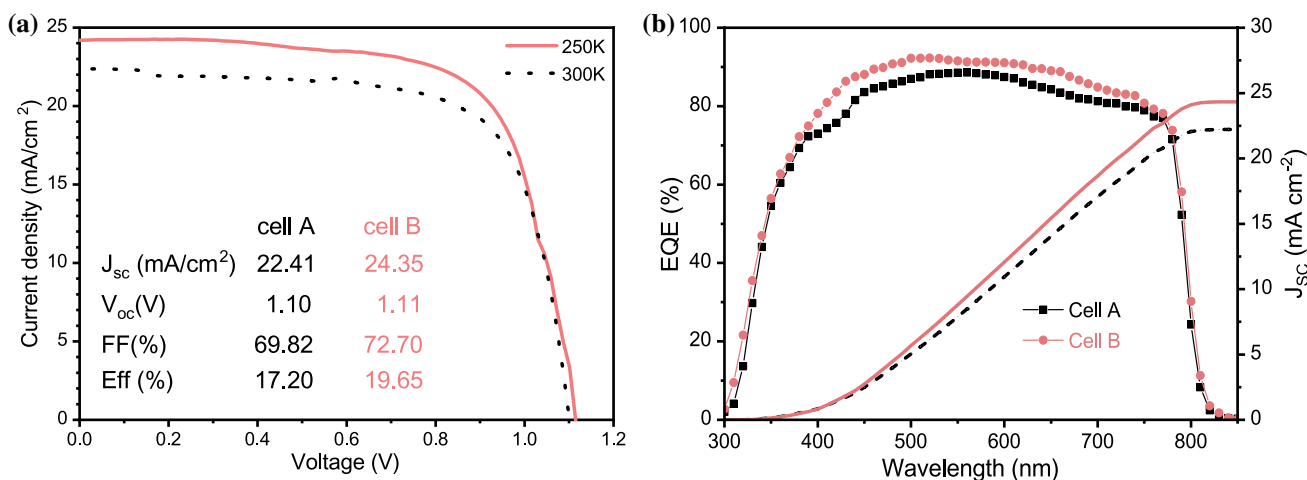


**Fig. 7** J–V curves of the champion cell in Cells A (with the anti-solvent at 300 K in the film preparation) and the champion cell in Cells B (with the anti-solvent at 250 K in the film preparation) (a), and the EQE comparison of the champion cell in Cells A with that in Cells B (b).

Fig. 6. Notably, Cells B have a better performance than Cells A, with the highest PCE of 19.65% and 17.2%, respectively. The  $V_{oc}$  and  $I_{sc}$  of Cells B are higher than those of Cells A, consistent with the better crystal quality of Film B than Film A, as discussed above. It may be noted that the fill factor (FF) of Cell A is obviously lower than that of Cell B, a deviation caused by the device fabrication process. However, even considering the effect of this FF deviation, the conversion efficiency of Cells B is still convincingly higher than those of Cells A.

Figure 7a shows the J–V curves of the respective champion cells in Cells A and Cells B, with the external quantum efficiency (EQE) comparison in Fig. 7b of the corresponding champion cells. The better performance of the champion cell in Cells B than that in Cells A is consistent with the above discussed observation and also supported by the better EQE of the cell.

## Conclusions

An approach of a simpler and more quantitatively controllable low temperature anti-solvent treatment has been introduced in the preparation of perovskite films. The perovskite films prepared with pure IPA anti-solvent treatment at 250 K have a larger grain size than those at 300 K. The enhanced grain size is a result of the suppressed nucleation rate due to the lower temperature at the nucleation stage. Also, the crystallinity of the films with anti-solvent treatment at 250 K is better than that at 300 K. With performance tests and analysis, the solar cells made from the films using anti-solvent treatment at 250 K have a higher conversion efficiency than at 300 K, convincingly reflecting the improved quality. Unfortunately, experiments at a temperature lower than 250 K failed in the spin-coating due to the too high viscosity, although further improvements at temperatures lower than 250 K are expected.

**Acknowledgments** We acknowledge the financial support by the National Natural Science Foundation of China (No 11874200 and 12204245).

**Data availability** Data will be made available on request.

**Conflict of interest** The authors declare that they have no conflict of interest.

## References

- G. Wang, D. Liu, J. Xiang, D. Zhou, K. Alameh, B. Ding, and Q. Song, Efficient perovskite solar cell fabricated in ambient air using one-step spin-coating. *RSC Adv.* 6, 43299 (2016).
- C. Li, Q. Guo, W. Qiao, Q. Chen, S. Ma, X. Pan, F. Wang, J. Yao, C. Zhang, and M. Xiao, Efficient lead acetate sourced planar heterojunction perovskite solar cells with enhanced substrate coverage via one-step spin-coating. *Org. Electron.* 33, 194 (2016).
- Y. Ren, B. Duan, Y. Xu, Y. Huang, Z. Li, L. Hu, T. Hayat, H. Wang, J. Zhu, and S. Dai, New insight into solvent engineering technology from evolution of intermediates via one-step spin-coating approach. *Sci. China Mater.* 60, 392 (2017).
- S. Pratap, F. Babbe, N.S. Barchi, Z. Yuan, T. Luong, Z. Haber, T.-B. Song, J.L. Slack, C.V. Stan, and N. Tamura, Out-of-equilibrium processes in crystallization of organic-inorganic perovskites during spin coating. *Nat. Commun.* 12, 5624 (2021).
- L. Ling, S. Yuan, P. Wang, H. Zhang, L. Tu, J. Wang, Y. Zhan, and L. Zheng, Precisely controlled hydration water for performance improvement of organic-inorganic perovskite solar cells. *Adv. Func. Mater.* 26, 5028 (2016).
- Y.-N. Zhang, B. Li, L. Fu, and L.-W. Yin, One-step-spin-coating route for homogeneous perovskite/pyrrole-C60 fullerene bulk heterojunction for high performance solar cells. *J. Power Sources* 419, 27 (2019).
- S. Chen, X. Xiao, B. Chen, L.L. Kelly, J. Zhao, Y. Lin, M.F. Toney, and J. Huang, Crystallization in one-step solution deposition of perovskite films: upward or downward? *Sci. Adv.* 7, eabb2412 (2021).
- K. Schötz, C. Greve, A. Langen, H. Gorter, I. Dogan, Y. Galagan, A.J. van Breemen, G.H. Gelinck, E.M. Herzig, and F. Panzer, Understanding differences in the crystallization kinetics between one-step slot-die coating and spin coating of MAPbI<sub>3</sub> using multimodal in situ optical spectroscopy. *Adv. Optic. Mater.* 9, 2101161 (2021).
- Y.-K. Ren, S.-D. Liu, B. Duan, Y.-F. Xu, Z.-Q. Li, Y. Huang, L.-H. Hu, J. Zhu, and S.-Y. Dai, Controllable intermediates by molecular self-assembly for optimizing the fabrication of large-grain perovskite films via one-step spin-coating. *J. Alloys. Compd.* 705, 205 (2017).
- M. Wang, Y. Feng, J. Bian, H. Liu, and Y. Shi, A comparative study of one-step and two-step approaches for MAPbI<sub>3</sub> perovskite layer and its influence on the performance of mesoscopic perovskite solar cell. *Chem. Phys. Lett.* 692, 44 (2018).
- N. Zhang, Z. Zhang, T. Liu, T. He, P. Liu, J. Li, F. Yang, G. Song, Z. Liu, and M. Yuan, Efficient and stable MAPbI<sub>3</sub> perovskite solar cells via green anti-solvent diethyl carbonate. *Org. Electron.* 113, 106709 (2023).
- F. Bisconti, A. Giuri, R. Suhonen, T.M. Kraft, M. Ylikunnari, V. Holappa, P. Biagini, A. Savoini, G. Marra, and S. Colella, One-step polymer assisted roll-to-roll gravure-printed perovskite solar cells without using anti-solvent bathing. *Cell Rep. Phys. Sci.* 2, 100639 (2021).
- S.H. Chang, W.-C. Huang, C.-C. Chen, S.-H. Chen, and C.-G. Wu, Effects of anti-solvent (iodobenzene) volume on the formation of CH<sub>3</sub>NH<sub>3</sub>PbI<sub>3</sub> thin films and their application in photovoltaic cells. *Appl. Surf. Sci.* 445, 24 (2018).
- Z. Wang, L. Liu, Y. Wang, Y. Ma, Z. Yang, M. Wan, H. Zhu, T. Mahmoudi, Y.-B. Hahn, and Y. Mai, Green antisolvent-mediators stabilize perovskites for efficient NiOx-based inverted solar cells with  $V_{oc}$  approaching 1.2 V. *Chem. Eng. J.* 457, 141204 (2023).
- W. Xu, Y. Gao, W. Ming, F. He, J. Li, X.H. Zhu, F. Kang, J. Li, and G. Wei, Suppressing defects-induced nonradiative recombination for efficient perovskite solar cells through green antisolvent engineering. *Adv. Mater.* 32, 2003965 (2020).
- X. Zhang, X. Li, L. Tao, Z. Zhang, H. Ling, X. Fu, S. Wang, M.J. Ko, J. Luo, and J. Chen, Precise control of crystallization and phase-transition with green anti-solvent in wide-bandgap perovskite solar cells with open-circuit voltage exceeding 1.25 V. *Small* (2023). <https://doi.org/10.1002/sml.202208289>.

17. G. Jang, H.C. Kwon, S. Ma, S.C. Yun, H. Yang, and J. Moon, Cold antisolvent bathing derived highly efficient large-area perovskite solar cells. *Adv. Energy Mater.* 9(36), 1901719 (2019).
18. J. Sin, H. Kim, M. Kim, M. Kim, J. Shin, J. Hong, and J. Yang, Anti-solvent treatment time approach to high efficiency perovskite solar cells with temperature of coating environmental. *Solar Energy Mater. Solar Cells* 250, 112054 (2023).
19. H. Zhang, C. Zhao, D. Li, H. Guo, F. Liao, W. Cao, X. Niu, and Y. Zhao, Effects of substrate temperature on the crystallization process and properties of mixed-ion perovskite layers. *J. Mater. Chem. A* 7, 2804 (2019).
20. Y.K. Ren, X.H. Ding, Y.H. Wu, J. Zhu, T. Hayat, A. Alsaedi, Y.F. Xu, Z.Q. Li, S.F. Yang, and S.Y. Dai, Temperature-assisted rapid nucleation: a facile method to optimize the film morphology for perovskite solar cells. *J. Mater. Chem. A* 5, 20327 (2017).
21. J.-W. Lee, H.-S. Kim, and N.-G. Park, Lewis acid–base adduct approach for high efficiency perovskite solar cells. *Acc. Chem. Res.* 49, 311 (2016).
22. Y. Yamada, T. Nakamura, M. Endo, A. Wakamiya, and Y. Kanemitsu, Near-band-edge optical responses of solution-processed organic–inorganic hybrid perovskite CH<sub>3</sub>NH<sub>3</sub>PbI<sub>3</sub> on mesoporous TiO<sub>2</sub> electrodes. *Appl. Phys. Express* 7, 032302 (2014).
23. N. Ashcroft and N. Mermin, *Solid state physics* (Saunders College, Philadelphia). Google Scholar 404 (1976).
24. H.H. Fang, R. Raissa, M. Abdu-Aguye, S. Adjokatse, G.R. Blake, J. Even, and M.A. Loi, Photophysics of organic–inorganic hybrid lead iodide perovskite single crystals. *Adv. Funct. Mater.* 25, 2378 (2015).
25. J.M. Frost, K.T. Butler, F. Brivio, C.H. Hendon, M. Van Schilf-gaarde, and A. Walsh, Atomistic origins of high-performance in hybrid halide perovskite solar cells. *Nano Lett.* 14, 2584 (2014).
26. B.J. Foley, D.L. Marlowe, K. Sun, W.A. Saidi, L. Scudiero, M.C. Gupta, and J.J. Choi, Temperature dependent energy levels of methylammonium lead iodide perovskite. *Appl. Phys. Lett.* 106, 243904 (2015).
27. C. Quarti, E. Mosconi, J.M. Ball, V. D’Innocenzo, C. Tao, S. Pathak, H.J. Snaith, A. Petrozza, and F. De Angelis, Structural and optical properties of methylammonium lead iodide across the tetragonal to cubic phase transition: implications for perovskite solar cells. *Energy Environ. Sci.* 9, 155 (2016).
28. P. Jing, J. Zheng, M. Ikezawa, X. Liu, S. Lv, X. Kong, J. Zhao, and Y. Masumoto, Temperature-dependent photoluminescence of CdSe-core CdS/CdZnS/ZnS-multishell quantum dots. *J. Phys. Chem. C* 113, 13545 (2009).

**Publisher's Note** Springer Nature remains neutral with regard to jurisdictional claims in published maps and institutional affiliations.

Springer Nature or its licensor (e.g. a society or other partner) holds exclusive rights to this article under a publishing agreement with the author(s) or other rightsholder(s); author self-archiving of the accepted manuscript version of this article is solely governed by the terms of such publishing agreement and applicable law.